The Mechanical Properties of Newly Developed Iron and Nickel-based Hardfacing Alloys for Industrial Applications

A Senior Project

presented to

the Faculty of the Materials Engineering

California Polytechnic State University, San Luis Obispo

In Partial Fulfillment

of the Requirements for the Degree

Bachelor of Science

by

Kristi Lucas

June 11, 2014

The Mechanical Properties of Newly Developed Iron and Nickel-based Hardfacing Alloys for Industrial Applications

---

Kristi Lucas

California Polytechnic State University

Materials Engineering Senior Project

Advisor: Professor Blair London

Corporate Sponsor: Scoperta Inc.

June 11, 2014

Acknowledgments

I would like to thank my senior project sponsor Scoperta Inc. for providing funding as well as the samples to make my project possible. In particular John Madok, Justin Cheney, and Jonathon Bracci from Scoperta provided me with the technical expertise on their hardfacing alloys that were tested for strength properties. I would also like to thank my advisor, Dr. Blair London, who provided weekly deadlines, guidelines and continued support throughout this process.

Abstract

Standard practice in the oil-drilling industry is to weld-deposit a hardfacing layer to the outside of a tool joint prolonging the life of the tool. These hardfacing layers are iron (steel)-based and nickel-based alloys. The main applications for the steel-based hardfacing alloys are for hardfacing, hardbanding, and non-magnetic hardbanding. The nickel-based hardfacing alloy application is a corrosion resistance weld overlay. Current hardfacing alloys do not have mechanical data due to the difficultly in producing samples suitable for mechanical testing. Microhardness and three-point bend testing were done to measure the alloys' mechanical properties. Samples from six hardfacing alloys were tested in three different forms: melted ingots, un-notched bend, and notched bend samples. Six different alloys designations were examined with varying amounts of Fe, B, C, Cr, Mn, Mo, Nb, Ni, Si, Ti, V, and W. The two main classes of these different alloys are ferritic and austenitic. Six small arc-welded ingots roughly 1 x 0.5 inches were produced for microhardness testing. The ferritic steel-based hardfacing alloy was the highest hardness measured at 62.3 HRC. The austenitic nickel-based hardfacing alloy was the lowest hardness measured at 30.3 HRC. Three-point bend testing was conducted on two different types of samples: un-notched and notched. The bend samples were fabricated by weld depositing a hardfacing alloy onto a steel plate. The thickness was achieved with three layers and three weld beads. Dimensions for the smooth and notched bend samples were completed with Electro Discharge Machine (EDM) and the steel base plate was machined off. The results from the three-point bend test highlighted the un-notched bend samples' increased strength. There was a correlation between hardness and strength. The ferritic steel-based hardfacing alloy that was the hardest had the highest bending strength at 1856 MPa (Modulus of Rupture). The softest austenitic nickel-based hardfacing alloy had the lowest strength at 1117 MPa. Overall, the hardfacing alloys displayed high strength values. Scanning Electron Microscopy was employed to examine fracture surfaces to determine fracture characteristics.

Keywords: Hardfacing alloy, three-point bending, microhardness, weld-deposit, Modulus of Rupture, Scanning Electron Microscope, Materials Engineering

Table of Contents

List of Figures

List of Tables

Introduction

Problem Statement

Hardfacing alloys are commonly used in many applications such as drilling equipment in oil mining. The hardfacing alloys produced by Scoperta Inc., (San Diego, CA) are designed to be wear-resistant when encountering abrasive oil sands. The problem is the wear-resistant coatings are weld-deposited onto the steel drill pipe components and have been known to crack in neighboring weld beads. Scoperta designs different alloy designations to increase the wear resistance of the hardfacing alloy in order to address the cracking in the weld beads. The goal of this project is to evaluate the bend strength of different weld-deposited alloys through three-point bend testing to measure the modulus of rupture (MOR) and image the fracture surface with a Scanning Electron Microscope (SEM).

Application: Oil Drilling

Once oil has been located beneath the earth's surface, the land is prepared for the oil-drilling rig (Figure 1). The oil-drilling rig consists of power systems, mechanical systems, rotating equipment, and a circulation system. The rotating equipment is enclosed in the casing of the rig.

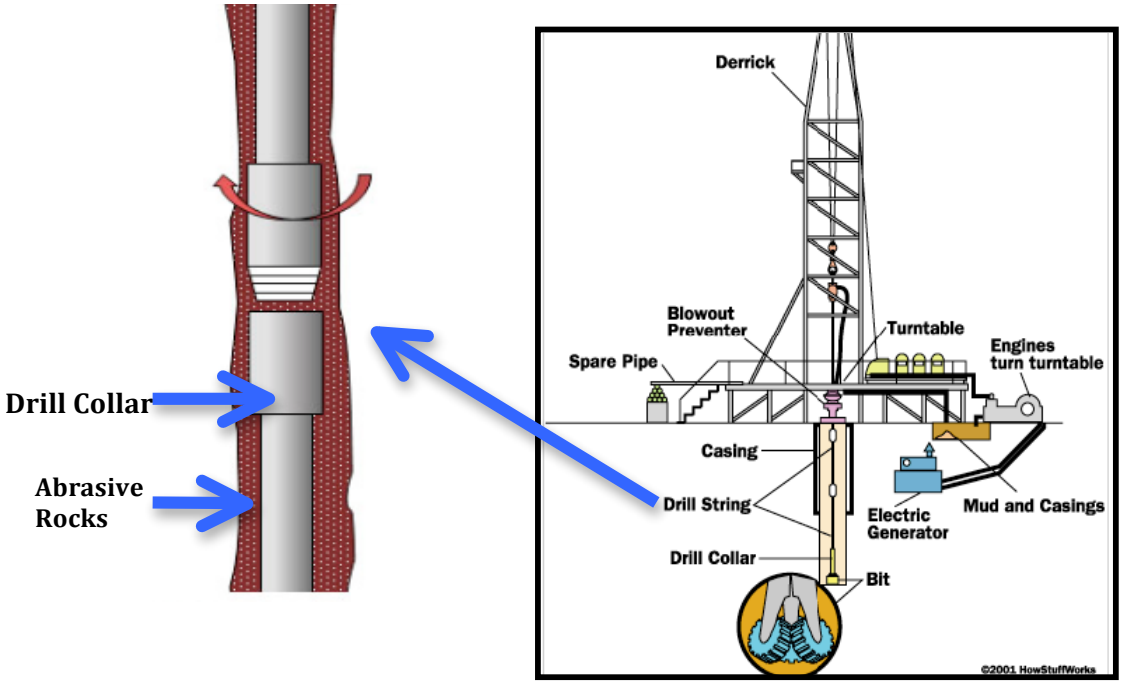

Figure 1: Oil-drilling rig schematic highlighting the drill collar[1].

The casing in Figure 1 is a large-diameter concrete pipe that lines the drill hole in order to prevent the hole from collapsing. Within the casing there is a drill string that consists of 10-meter sections of drill pipes that are connected together. A larger diameter, heavier pipe fits around the drill pipe called a drill collar[1]. As the hole becomes deeper, more sections of drill string are added[2]. Clogging of the drill bit during the drilling process is prevented with the circulation system. The drill string and drill collar need to be fabricated from wear-resistant material due to the abrasive rocks and sands that they encounter in the drilling process.

Hardfacing

Hardfacing is the welding of a sacrificial layer of a hard, wear-resistant metal to a non-wear-resistant base metal[3] (steel most commonly). Hardfacing alloys are applied to the critical wear areas of a component or a tool[4]. The application of welding the sacrificial layer to a base material for a corrosion resistant weld overlay can be seen in Figure 2.

Figure 2: Corrosion weld overlay being applied to a base metal to increase the wear resistance [5].

The sacrificial layer of hardfacing material is usually done to prolong the life of the structural component[6]. The layer applied is designed to wear at a slower rate than the original alloy. Hardfacing alloys are used in harsh wear environments and are deposited through two main processes: metal-inert gas welding and twin-wire arc spray[6]. Small cracks can appear in the weld section when a hard, brittle alloy is applied as the sacrificial layer[7]. But if cracking occurs through the hardfacing alloy it could possibly lead to failure of the part. Applications that utilize hardfacing alloys include: mill hammers, digging tools, extrusion screws, cutting shears, and parts of earthmoving equipment[8].

Conventional hardfacing materials are also referred to as weld overlays[9]. A weld overlay can also restore the original dimensions of the component or essentially repair a damaged part. Weld overlay is different than general welding because it applies a corrosive or hardfacing layer onto the parent material[9]. The weld overlay provides protection against corrosion and helps reduce material wastage on the component, which can reduce the cost of replacing parts frequently due to wear.

Hardfacing alloys can be differentiated into five general categories, which include: buildup alloys, metal-to-metal wear alloys, metal-to-earth abrasion alloys, tungsten carbide, and nonferrous alloys[8]. On a microstructural level, hardfacing alloys consist of hard phase precipitates. These hard phase precipitates that form in iron, nickel, or cobalt-base alloy matrices include borides, carbides, or intermetallics[8].

Iron-Base Hardfacing Alloys

Iron-based hardfacing alloys are beneficial due to their low cost and range of properties. The iron-based hardfacing alloys are divided into different classes depending on the composition. The main classes are pearlitic steels, austenitic steels, martensitic steels, and high alloy steels[8]. The pearlitic steels are considered to be low alloy steels that contain generally less than 0.2% C (Table I). The weldability of pearlitic steels can be achieved by altering the composition slightly. This particular group of alloys tends to have low hardness (25 to 37 HRC), high impact resistance, and excellent weldability. Austenitic steels contain the addition of manganese in order to stabilize it. This addition of manganese provides the austenitic steels with high strength due to the interaction of carbon and manganese atoms. In order to only form the austenitic phase, manganese increases carbon solubility at lower temperatures and promotes carbon supersaturation[8]. Austenitic steels are considered to be metastable, which can delay phase transformations when the steel is cooled slowly or reheated. As a solution, the majority of the austenitic steel is submerged under water during the welding process in order to keep the part as cool as possible[8]. Martensitic steels are engineered to form the martensitic phase on the weld deposit upon normal air-cooling conditions. Typically, the carbon content can range up to 0.7% for these steels and have a hardness range of 45 to 60 HRC (Table I). Molybdenum, tungsten, nickel, and chromium (up to 12%) are added to increase hardenability. To increase the weldability of martensitic steels, manganese and silicon are added[8]. In mildly corrosive environments, slight modifications to the alloying elements, such as adding niobium or vanadium, are done to prevent corrosion[8].

Table I. Compositions and Hardness Values for Buildup Weld Overlay for Iron-Based Hardfacing alloys[8]

Alloy	Compositions wt%							Hardness (HRC)
	Fe	Cr	C	Si	Mn	Mo	Ni	
Pearlitic	Bal.	2.0	0.1	1.0	1.0	1.5	…	37
Austenitic	Bal.	4.0	0.8	1.3	14.0	…	4.0	18
Martensitic	Bal.	6.0	0.7	1.0	1.0	1.0	…	59

Nickel-base Hardfacing Alloys

Similar to iron-base hardfacing alloys, nickel-base hardfacing alloys can also be separated into different groups depending on their alloying elements. The three different groups are boride-containing alloys, carbide-containing alloys, and Laves phase-containing alloys[8]. The boride-containing nickel-base alloys were originally produced as spray-and-fuse powders[8]. The other alloying elements besides nickel in this group are chromium, boron, silicon, and carbon. The boron content can range from 1.5 to 3.5% and up to 16% for chromium content (Table II). The hardness in the higher chromium alloys can be attributed to the large amount of boron, which forms hard chromium borides[8]. The boride-containing nickel-base alloys have the most complex microstructure out of all the hardfacing alloys. This group of alloys exhibits excellent resistance to abrasion because of the dispersed borides and carbides in the microstructure[8]. Another group is the carbide-containing alloys, an up and coming alternatives to cobalt-base hardfacing alloys. This is because the nuclear power plants that used cobalt- base hardfacing alloys discovered that they are a source of highly radioactive ^{60}Co isotope[8]. Cobalt-base hardfacing alloys were originally preferred for their high weldability over the carbide-containing nickel-base hardfacing alloys. Recently, it has been revealed that the carbide-containing nickel-base hardfacing alloys that have nickel, chromium, molybdenum, cobalt, iron, tungsten, and carbon have better weldability than before[8]. The last group of nickel-base hardfacing alloys is Laves phase alloys. These alloys can be welded easily using gas-tungsten arc welding and have excellent metal-to-metal wear resistance[8].

Table II. Compositions in Weight Percent of Nickel-base Hardfacing Alloys[8]

Alloy	Composition wt%								
	Fe	Cr	Mo	W	Si	C	B	Co	Ni
Boride-containing alloys (Alloy 40)	1.5	7.5	…	…	3.5	0.3	1.5	…	Bal
Carbide-containing alloys (Alloy N-6)	3.0	29.0	5.5	2.0	1.5	1.1	0.6	3.0	Bal
Laves phase containing alloys (T-700)	…	16.0	33.0	…	3.5	…	…	…	Bal

Hardbanding

Hardbanding is the process where a hardfacing material is welded onto tool joints for underground drilling[10]. Hardbanding will increase the tool life of the drill joint by using weld beads that wrap around the outer diameter of the joint. The weld beads are typically applied using gas metal arc welding and can be several up to several inches wide (Figure 3). Another form is non-magnetic Hardbanding where the Hardbanding material is applied to a base material that is non-magnetic[11]. This type of Hardbanding can be applied even over layers of stainless steel. The non-magnetic Hardbanding material can be directly applied to a non-magnetic drill collar, like the one seen in Figure 3.

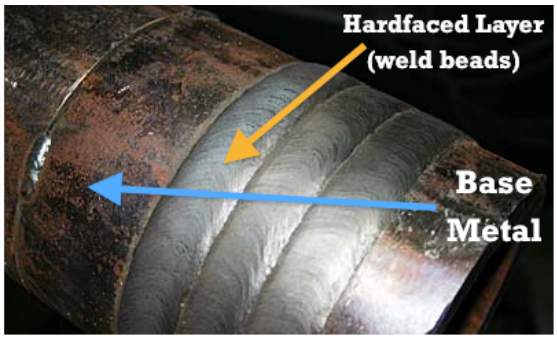

Figure 3: Three weld beads on a base metal drill joint for underground drilling in the oil industry[12].

Welding a Hardfacing Layer

With the intention to apply the hardfacing layer to the base material, a wide range of welding processes can be used. This weld allows a high strength bond to be made between the weld overlay and the component, providing protection to the base material[13]. Three types of processes can be used to weld a hardfaced layer are Tungsten Inert Gas (TIG) welding, manual metal arc welding, and Plasma-Transferred Arc (PTA) welding. TIG welding is an arc that is struck between a non-consumable tungsten electrode and the component (Figure 4).

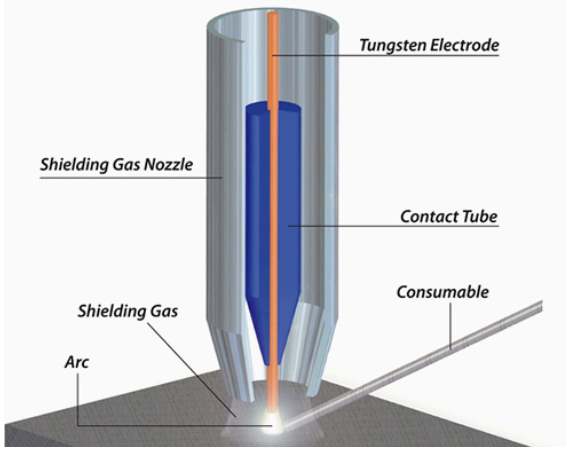

Figure 4: TIG welding schematic for applying hardfacing alloys on a substrate[13].

The electrode, the arc, and the weld pool are protected from the atmosphere with an inert shielding gas. Some advantages of this type of welding are manual and automated operation, and low dilution[13]. Dilution is the mixing of the base metal and weld metal during the weld depositing process. The objective is to keep the dilution low with the purpose to obtain optimal properties in the hardfacing layer[14]. Manual operation enables the operator to have good control over the welding arc. The process could also be automated, so that the component moves relative to the welding torch. Another type of welding is manual metal arc welding. This is the process of where an arc is drawn between a coated consumable electrode and component and where the metallic core-wire is melted and then transferred to weld pool as molten drops (Figure 5A). Some advantages of this type of welding include a lower cost, more portability, which makes it ideal for repairs. PTA welding has a highly concentrated heat source from the tungsten electrode (Figure 5B). Some advantages of PTA welding are it is highly automated, has high powder utilization, low dilution, and can weld a wide range of hardfacing materials[13]. A high degree of reproducibility of weld overlays can be achieved due to the high level of automation from the PTA process[13].

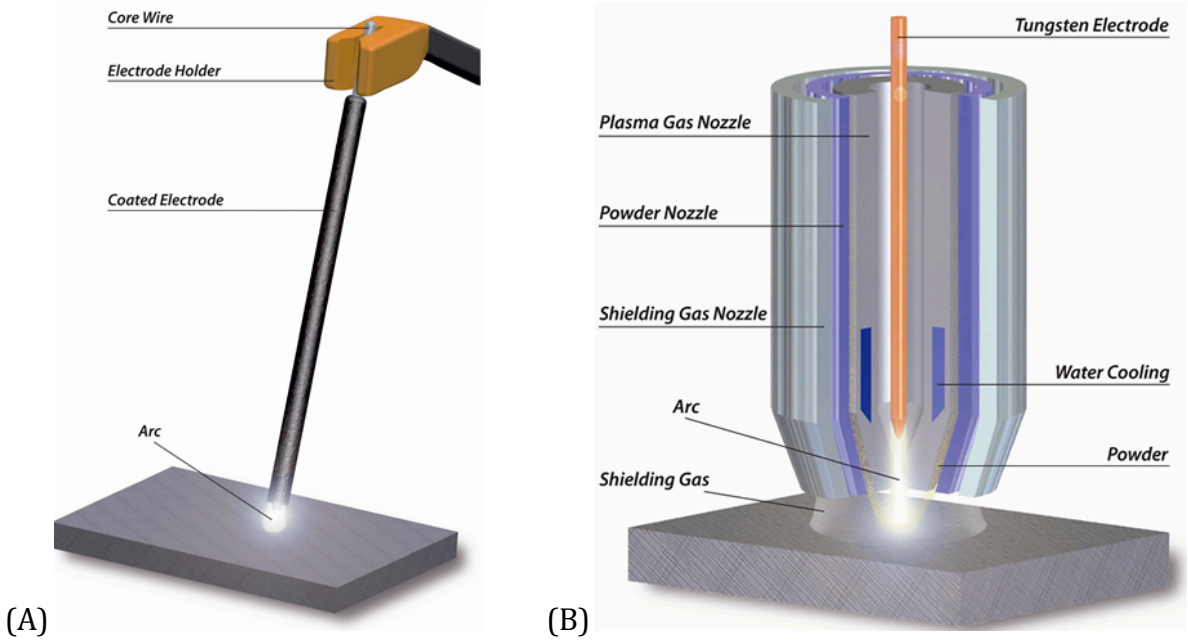

Figure 5: (A) Manual Metal Arc welding schematic and (B) PTA welding schematic for applying hardfacing alloys[13].

Three-Point Bend Test

A way to measure the strength of different materials can be done through a bend test. A bend test can also be referred to as flexure testing. A bend or flexural test is commonly done on brittle materials [15]. Samples are produced in a rectangular beam shape and placed in the testing position between the support and loading pins (Figure 6).

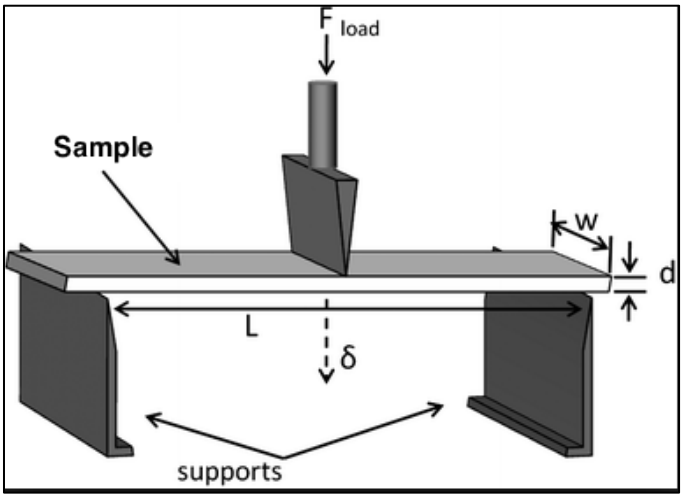

Figure 6: Example of bending under a three-point bend arragnement[16]**.**

During a bend test, the sample experiences two types of stresses. Along the top of the sample, it experiences compression stress and the bottom of the sample experiences tension stress (Figure 7).

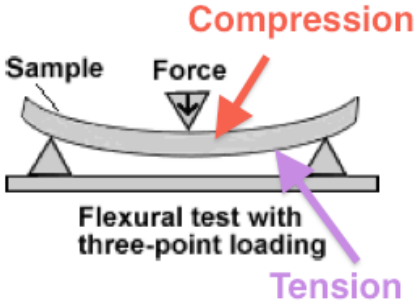

Figure 7: Three-point bend sample experiencing compression and tension stresses under a given load[17].

Due to the opposing stresses, a shear stress is formed along the midline of the sample[17]. The goal of a bend test is for sample to fail due to either compression or tensile stresses, not shear stress. In order to ensure that occurs, the span (S) to depth (d) ratio is controlled[17]. Studies have shown that an s/d ratio of 16 is an acceptable ratio in order to keep the shear stress low enough for tensile or compressive failure[17]. As the sample experiences different stresses during the bend test, a stress distribution diagram is produced (Figure 8).

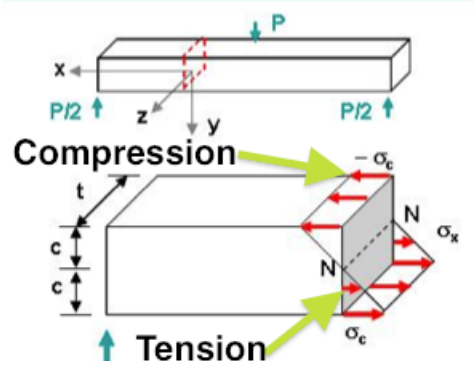

Figure 8: Stress distribution of compression and tension stress can be seen from the red arrows[15].

In this figure, the sample is cut in half in order to exemplify the compression and tension stresses during the bend test. The results of the bend test produce a stress-strain curve or load-displacement curve (Figure 9). As the sample has the load applied, elastic and plastic deformation can take place during beam deflection.

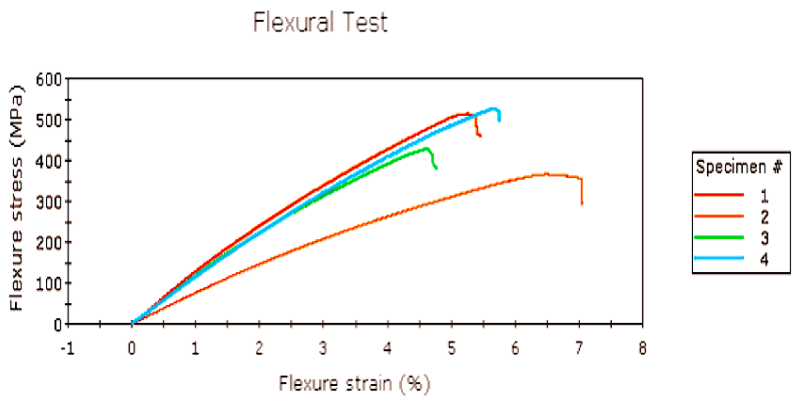

Figure 9: An example of the output of a bend test displaying stress and strain[15].

In Figure 9, the brittle samples experience a linear stress- strain behavior when undergoing loading. For brittle materials that have a linear stress-strain relationship, fracture stress as the bending moment (M) times half the specimen length (c) and then divided by the moment of inertia (I)[14]. The fracture stress in bending is called the bend or flexure strength. This calculated fracture stress, σ_f, should be equivalent to the maximum point on the stress-strain graph in Figure 9. Since this is a bend test of a brittle material, it is expected that the sample will have a sharp break downwards at the fracture point.

This fracture stress of the brittle material that is calculated in bending is equivalent to the modulus of rupture (MOR)[16]. Brittle materials have higher strength in compression than tension, which leads the sample to fail under bending due to weaker tensile stresses along the opposite side to the direction of the load applied[15].

Project Justification

It can cost over $40 million a year for the oil industry to replace damaged parts and to hire the labor to do so[17]. In order to increase the wear-resistance of hardfacing alloys, Scoperta has designed specialty hardfacing alloys to increase the toughness of the main components. These newly developed alloys have been characterized with respect to composition, microstructure and ability to be weld-deposited, but only limited mechanical properties, such as hardness are available. It is important to measure baseline mechanical properties of these alloys with the intention to predict the behavior of other similar hardfacing alloys that Scoperta may develop in the future.

Procedure

Three types of samples were produced, an ingot, an un-notched rectangular beam, and a notched rectangular beam (bend samples). These samples vary in compositions of alloying elements depending on the type of alloy, iron-based or nickel-based. The samples can be divided into different classes such as, Ferritic and Austenitic (Table III). The only nickel-based alloy in that was tested is NickoShield 100 (NS 100) while the other five alloys are iron-based.

Table III. Compositions of the Six Different Hardfacing Alloys for Microhardness and Three-point Bend Testing

Alloy Designation	Class	Compositions wt%											
		Fe	B	C	Cr	Mn	Mo	Nb	Ni	Si	Ti	V	W
H7	Ferritic	Bal.	0.85	0.85	5.75	0.30	0	4.60	0	0.60	0.20	2.75	10.80
350XT	Ferritic	Bal.	1.50	0.90	5.00	1.00	1.00	4.00	0	0.40	0.40	0.50	0
P21-X9	Ferritic	Bal.	0	1.07	5.00	1.20	0.75	0	0	0.75	3.00	0	0
P8-X11	Austenitic	Bal.	0	1.50	16.50	10.00	0	3.00	2.50	0	0.20	0.50	4.00
AHB35	Austenitic	Bal.	0	3.00	5.00	10.00	0	4.00	0	0	0.20	0.50	5.00
NS 100	Austenitic	0	0.40	0	26.70	0	12.70	0	Bal.	0	0	0	0

Three- Point Bend Test

Sample Preparation: Un-notched Bend Samples

The un-notched bend samples were weld-deposited onto a plate that was 3″x 6″x 1″. The shielding gas that was used for each sample was 100% argon with a travel speed of 7 inches per minute (imp). A36 steel was used for Ferritic samples and 304 stainless steel was used for austenitic samples. The Ferritic alloys include, H7, 350XT, and P21-X9. The austenitic alloys were the P8-X11, AHB35, and NS100. The thickness of the samples was achieved with three layers and three weld beads. One bead was one inch wide, four inches long and three millimeters thick. After three layers the total thickness was about eight millimeters. These samples were then water jet cut into specific dimensions (Figure 10). The steel base metal was machined off with the purpose to test only the hardfacing layer. Due to the brittle characteristics of hardfacing alloys,

only four out of the six were successfully made (H7, 350XT, P21-X9, and P8-X11), while the AHB35 and NS100 both cracked during the welding and cutting processes.

A)

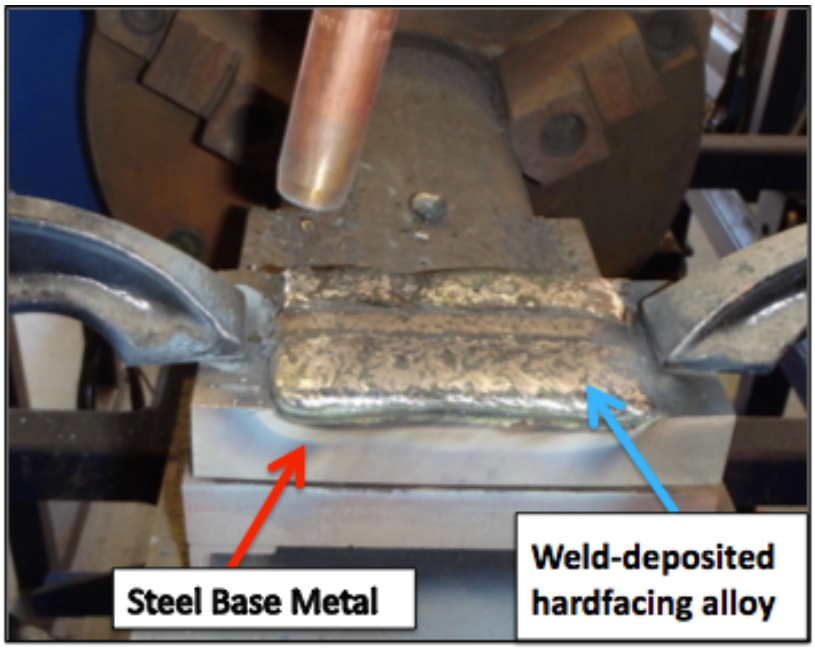

B)

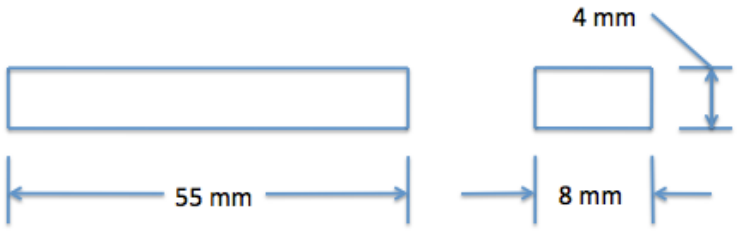

Figure 10: A) Weld-deposit of hardfacing alloy to steel base. B) Dimensions for 3-point bend test samples after cutting process.

Sample Preparation: Notched Bend Samples

Due to the cracking of the AHB35 and NS100 for the un-notched samples, notched samples were fabricated to test all six alloys. The notched samples were prepared with the same procedure as the un-notched samples. These samples were then water jet cut into specific dimensions with a V-shaped notched located near the center (Figure 11). All samples were notched with a 2.0 mm broach. All six alloys had successful samples produced. It should be noted that there were visible surface cracks and porosity present on few of the samples (AHB35, NS100, and H7). The main difference between the notched and un-notched bend samples is that the base material is still welded to the weld-deposited hardfacing alloy. The thickness of the weld-deposit layer and the steel base varied slightly depending on the alloy (Table IV).

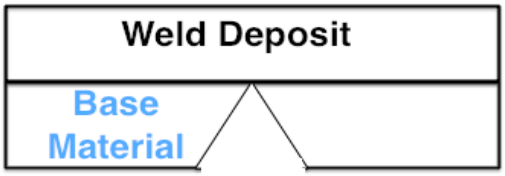

Figure 11: Notch 3-point test sample schematic.

Table IV. Notched Bend Test Sample Dimensions

Sample	Total Thickness (mm)	Base Thickness (mm)	Milled off Base (mm)
H7-2	12.1	4.7	1.9
H7-3	11.9	4.9	2.8
AHB35-1	11.4	3.3	1.1
AHB35-2**	11.4	2.7	0.7
AHB35-3	11.4	2.3	0.3
NS100-1	12.7	4.8	2.8
NS100-2	12.7	5.6	3.6
NS100-3	12.7	4.6	2.6
P21-X9-1	11.3	4.3	2.3
P21-X9-2	11.2	1.9	0.0
350XT-1	11.2	2.9	0.8
350XT-2	11.2	2.8	0.8
P8-X11-1	11.3	4.3	2.3

**Notch moved 6mm off center to avoid existing crack in weld

Testing Procedure: Un-notched and notched bend samples

Un-notched and notched bend samples were loaded into a three-point bend test fixture using an Intsron 3369 testing machine (50 kN, 10,000 lb capacity). Each alloy sample was loaded between the two support pins and loading pin (Figure 12). Sample dimensions were then entered into the computer program and a load was applied to the sample. The load was applied until the sample fractured. Load, strength, and extension data was collected.

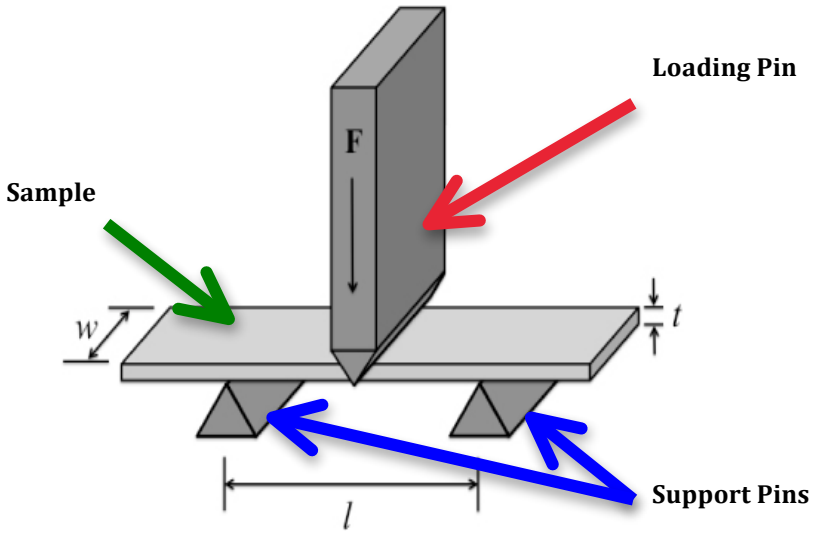

Figure 12: Three-point bend test set up for both un-notched and notched samples[14].

Scanning Electron Microscope (SEM) Examination

Sample Preparation

Once the un-notched bend test sample had fractured, the fracture surface was cut off using a low-speed saw. Each fracture surface sample was then cleaned. Each sample was placed into an acetone solution in a beaker and then placed into a ultrasonic cleaning bath of water where vibrations would gently shake dirt off the sample for five minutes. The cleaning process removes any impurities or dirt left on the surface from the cutting process. SEM samples were then dusted using an air gun. Once samples were clean and dust free, each was mounted onto a mounting stage using carbon tape.

Micro- Hardness

Sample Preparation: Ingot

The six ingot samples were produced from a weld wire that was cut into four-inch sections placed into copper molds and then arc melted together. To ensure that the ingot samples were homogeneous, each ingot was melted three or four times. A tungsten electrode produced an arc while the chamber is filled with argon gas melted the ingot.

Testing Procedure

The six different alloy ingots were cut, mounted in Bakelite, and final polished. The alloys were microhardness tested while mounted at a load of 500 gram-force using a Micromet 2100

Series microhardness testing machine. The alloys were tested in ten random locations along the longitudinal direction. The values were recorded from measuring the length each of the diagonals from the pyramid shape of the indenter. The values were measured in Vickers and converted to HRC.

Results

Three- Point Bend Test

Three-point bend data was collected for un-notched and notched samples. The un-notched data measured the strength of the 350XT,P21-X9, P8-X11, and H7 alloys (Figure 13). The values of Modulus of rupture strength and extension for the un-nothced four alloys tested are displayed in Table V.

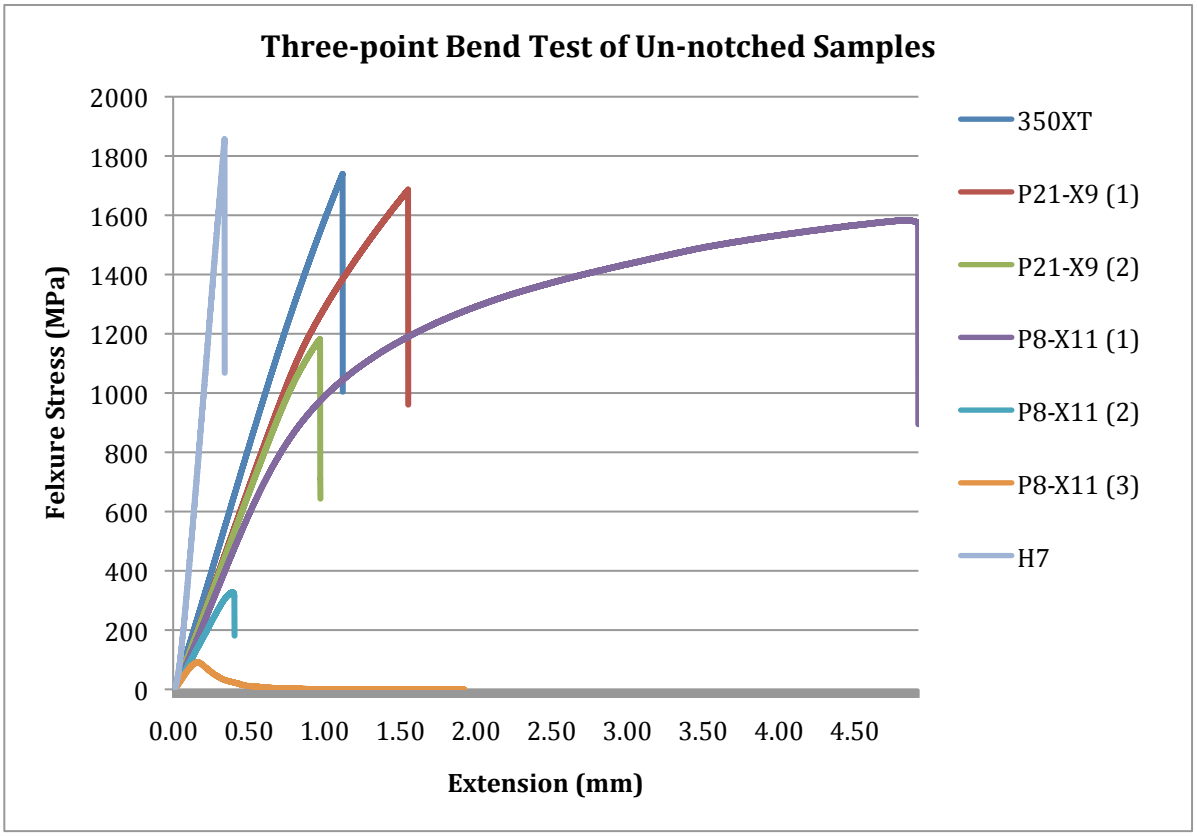

Figure 13: Three-point bend test of un-notched samples.

Table V. Summary of Extension and Modulus of Rupture Strength Values for Un-notched Samples

Alloy Designation	Extension at Maximum Stress (mm)	Modulus of Rupture Strength (MPa)
H7	0.30	1856
350XT	1.10	1739
P21-X9 (1)	1.53	1686
P21-X9 (2)	0.95	1182
P8-X11 (1)	4.86	1583
P8-X11 (2)	0.37	328
P8-X11 (3)	0.15	91.5

The greatest strength values for H7, 350XT, P21-X9, and P8-X11 are 1859 MPa, 1739 MPa, 1686 MPa, and 1583 MPa respectively. Samples two and three for the P8-X11 alloy failed prematurely due to possible to cracks between weld layers, which explain the low strength and extension values and were therefore not representative of the P8-X11 alloy. The H7 had the shortest extension at 0.3 mm and the P8-X11 had the largest extension at 4.86 mm. The H7 alloy had the highest modulus of rupture strength value.

The notched bend samples were divided into two plots, one for ferritic samples and the other for austenitic samples. The ferritic samples include H7, 350XT, and P21-X9 alloys (Figure 14). The P21-X9 exemplified the highest strength at 1284 MPa. The greatest strengths for the H7 alloy and the 350XT were 830 MPa and 949 MPa, respectively. The austenitic samples for notched three-point bend testing included the P8-X11, AH35, and NS100 alloys (Figure 15). The highest strengths for the AHB35, P8-X11, and NS100 are 978 MPa, 863 MPa, and 1117 MPa, respectively. The first sample for NS100 demonstrated the largest extension of 3.67 mm. The AHB35 hardfacing alloy had a unique U-shaped curve after the main failure of the sample. It was also noted that the NS100 alloy and some of the AHB35 alloy notched samples did not fracture into two complete pieces and displayed plastic deformation. Notched ferritic and austenitic samples are summarized in Table VI, which included values for extension at maximum stress and modulus of rupture strength values for each hardfacing alloy.

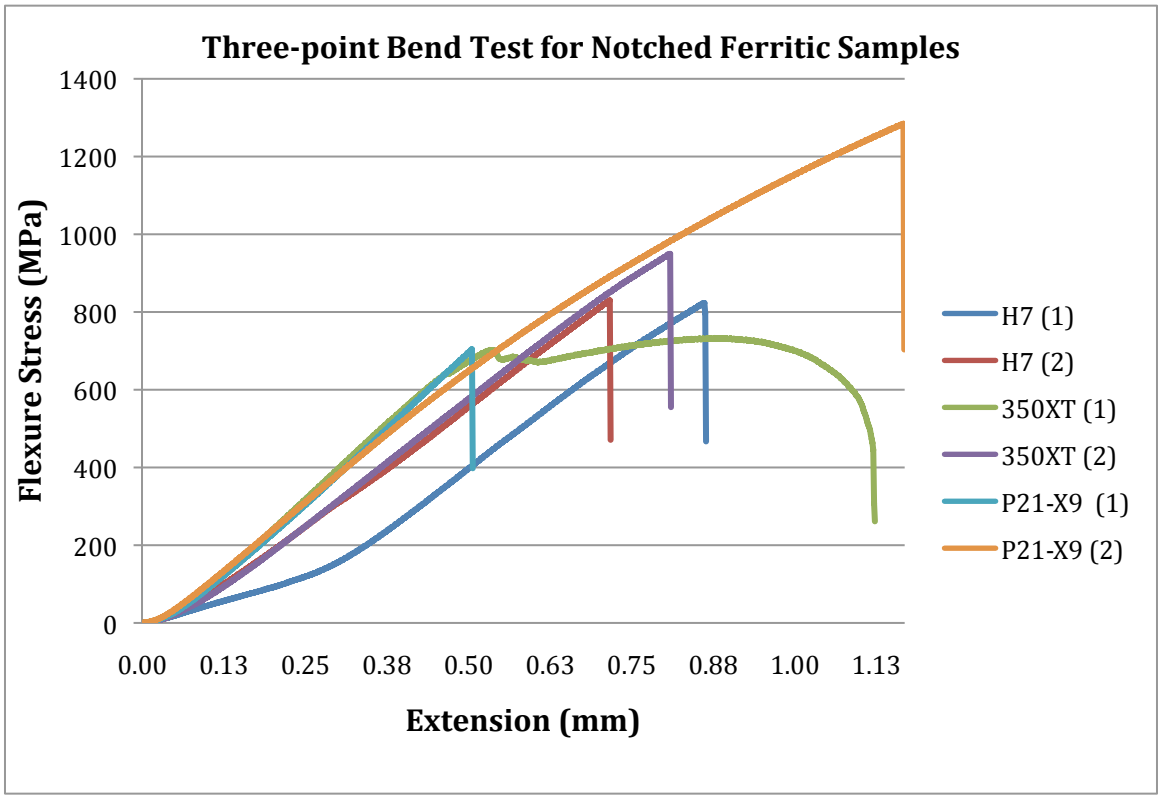

Figure 14: Three-point bend test for notched ferritic samples.

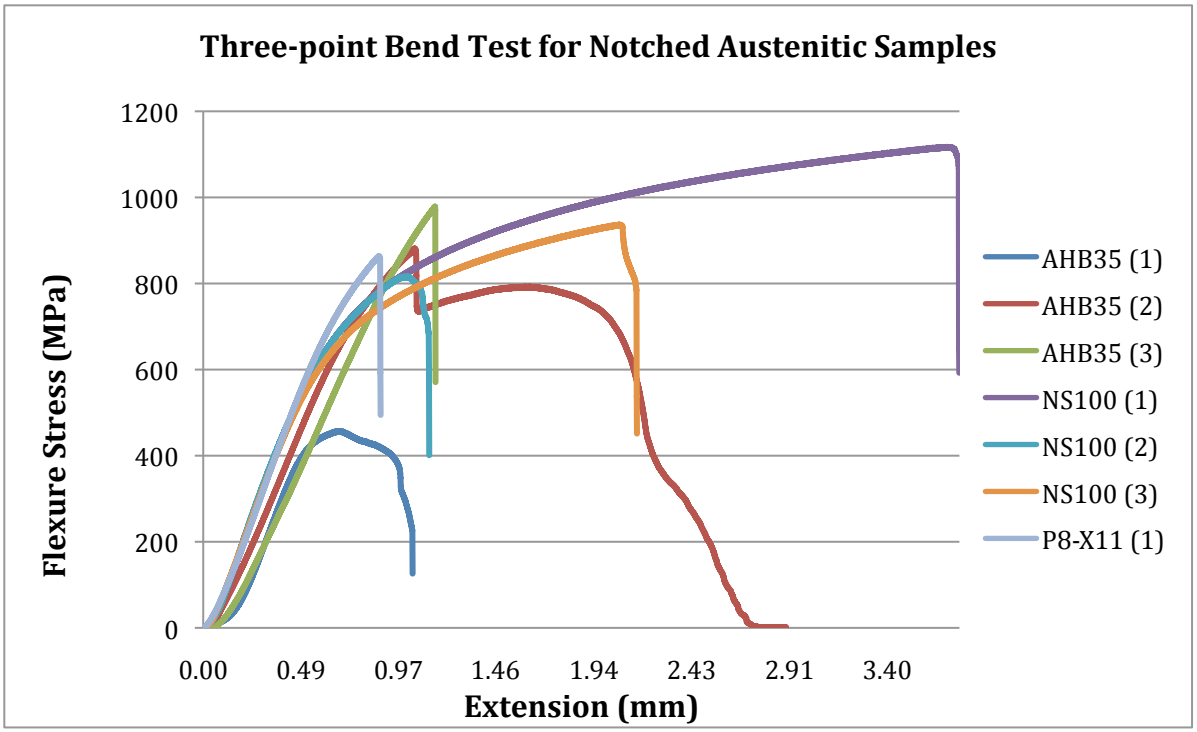

Figure 15: Three-point bend test results for notched austenitic samples.

Table VI. Summary of Extension and Modulus of Rupture Strength Values for Notched Samples

Alloy Designation	Extension at Maximum Stress (mm)	Modulus of Rupture Strength (MPa)
H7 (1)	0.67	823
H7 (2)	0.64	830
350XT (1)	0.83	733
350XT (2)	0.75	949
P21-X9 (1)	0.44	704
P21-X9 (2)	1.14	1284
P8-X11 (1)	0.82	863
AHB35 (1)	0.53	457
AHB35 (2)	0.98	881
AHB35 (3)	1.02	978
NS100 (1)	3.67	1117
NS100 (2)	0.97	816
NS100 (3)	2.03	936

Scanning Electron Microscope (SEM)

SEM imaging was completed on the fracture surfaces for the un-notched three-point bend test, which included the 350XT, H7, P21-X9, and P8-X11 alloys. The notched three-point bend test samples were not imaged with an SEM. Multiple SEM images were taken of each alloy at relatively high magnifications (approximately 2000X magnification), but all were uniform throughout the surface of the fracture. A representative image for each alloy's fracture surface can be seen in Figure 16. Imaging was done at the crack initiation site that failed under the given load. For more additional SEM images of each alloy that fractured in bend testing refer to Appendix A.

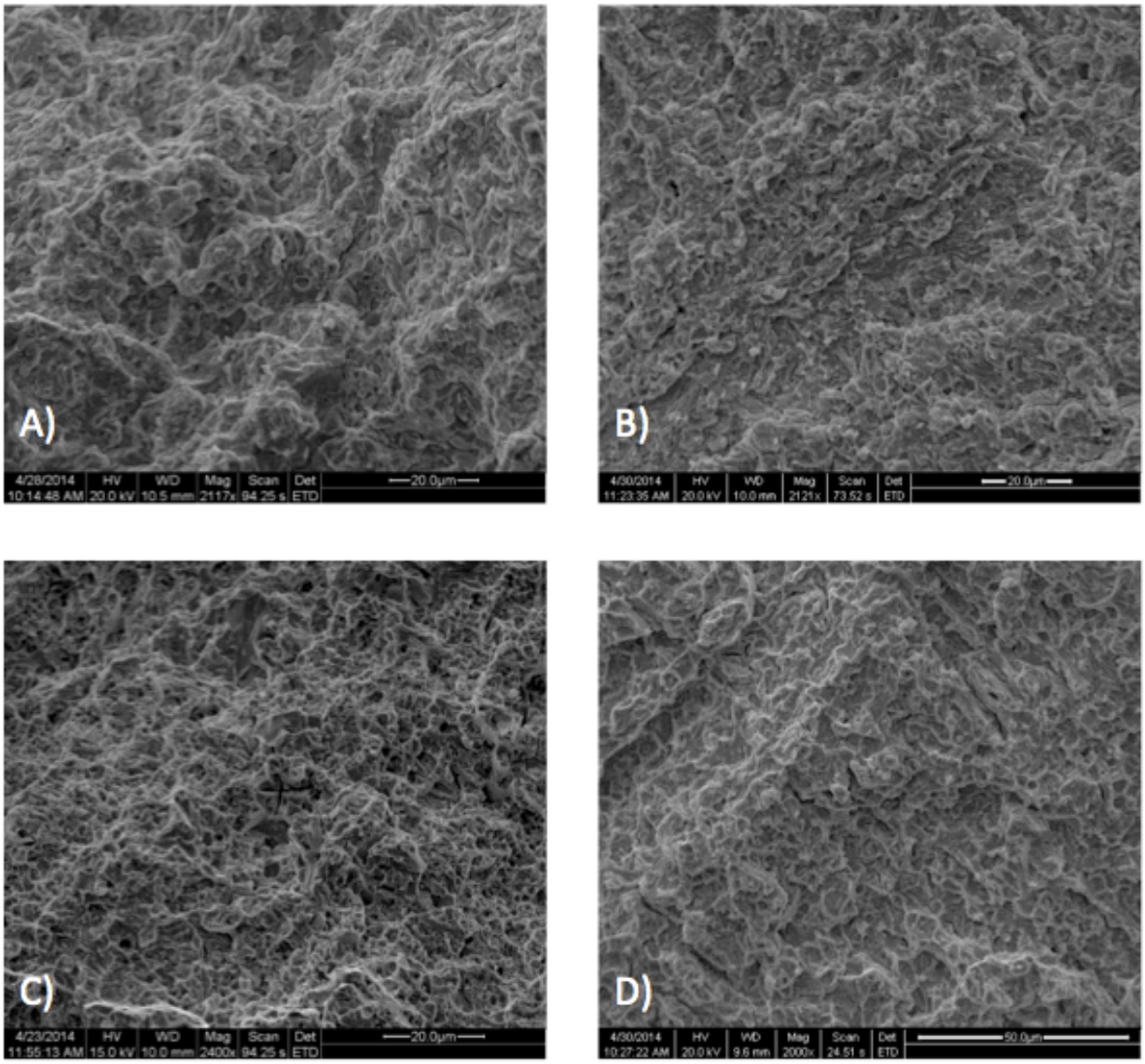

Figure 16: SEM images of the fracture surfaces of the four un-notched samples A) H7 at 2121X magnification B) 350XT at 2117X magnification C) P21-X9 at 2400X magnification and D) P8-X11 at 2000X magnification.

Microhardness

Microhardness was done on each hardfacing alloy. There was a wide range of hardness values that were recorded. Ten readings were taken on each alloy (Appendix B). A box plot was generated from the ten readings taken from the test (Figure 17).

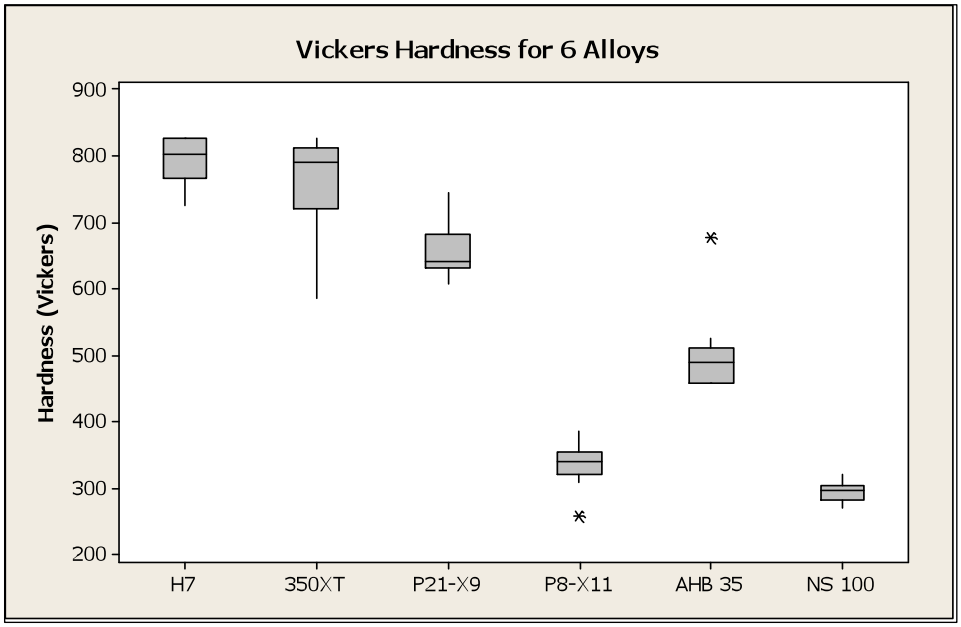

Figure 17: Box plot for microhardness of all 6 hardfacing alloys.

On the box plot the horizontal line in the middle of each grey box indicates the mean for that particular alloy. The H7 alloy was the hardest at 795 Vickers and the softest was NS100 at 294 Vickers. The asterisks on P8-X11 and AHB35 alloys signify an outlier was present during data collection. NS100 had the smallest range within the data collected at 49.5 and 350XT had the largest range at 239.5. The mean, standard deviation, and HRC values are displayed in Table VII. The standard deviations were high and had a wide range of variance. The ferritic alloys (H7, 350XT, and P21-X9) had the highest hardness, whereas the austenitic alloys (P8-X11, AHB35, and NS100) had the lowest hardness.

Table VII. Mean, Standard Deviation and HRC Values for H7, 350XT, P21-X9, P8-X11, AHB 35, and NS 100 Alloys

Alloy	Vickers Mean	Standard Deviation	HRC
H7	794.7	34.3	62.3
350XT	760.4	76.5	60.9
P21-X9	657.1	40.0	56.8
P8-X11	334.1	33.9	35.0
AHB35	502.8	65.7	49.8
NS100	294.6	15.57	30.3

Discussion

Three-Point Bend Test

The shape of the plot from the un-notched bend samples was expected. The linear-elastic slope up to a sharp turn down at the fracture point is characteristic of a brittle material. The P8-X11 sample 1 showed the most ductility due to the largest extension of 4.86 mm. The sample showed evidence of plastic deformation after fracture. The other alloys did not have this level of ductility present. P8-X11 samples 2 and 3 had the lowest strengths, which signifies that these samples failed prematurely due to cracks were present within the sample prior to testing possibly between the weld layers from the welding and cutting processes.

The notched bend data had uniquely shaped curves. The AHB35 had the most unique shaped data with bumps and curves throughout. These samples still had the hardfacing alloy that was weld-deposited to the base steel metal. The steel base could have had an effect on the hardfacing alloy being tested. Another factor is the stress concentration of the V-shaped notch. The properties of A36 steel and 304 stainless steel are different and could lead to inconsistent strength values if the notch did not get machined all the way through the base material.

When comparing both sets of results from the un-notched and notched bend tests, the strength values of the un-notched are higher and more representative of the actual strength of the hardfacing alloy. For example, the H7 alloy had an un-notched strength value of 1856 MPa and a notched strength value of 830 MPa. The difference between the two values can be seen by the ratio in Table VIII, which can be attributed to the stress concentrations from notch. A stress concentration factor, k_t, was calculated for each alloy using a 45 degree notch angle[21].

Table VIII. Comparison of Un-notched and Notched Strength Values for H7, 350XT, P21-X9, and P8-X11 Alloys

Alloy	Un-notched Strength (MPa)	Notched Strength (MPa)	Ratio of Un-notched and Notched Strengths	Calculated Stress Concentrations Ratio (k_t)
H7	1856	830	2.2	1.32
350XT	1739	949	1.8	1.78
P21-X9	1686	1284	1.3	2.14
P8-X11	1583	863	1.8	1.38

The k_t values for each were relatively similar to the ratios of un-notched to notched strengths, which demonstrate that the notched test was an acceptable way to measure Modulus of Rupture. The notched bend strengths are more representative than the un-notched bend strengths for the level of stress the hardfacing alloy can withstand during application when welded to a base drill collar.

Scanning Electron Microscope (SEM)

SEM images taken of all four un-notched hardfacing alloys that were bend tested showed brittle fracture characteristics, which was expected for hardfacing alloys (Figure 18). These SEM images are taken at higher magnifications (approximately 5000X magnification). At higher magnifications, fracture characteristics are more easily defined. Flat plate-like areas denote brittle characteristics and pockets or pores denote ductile characteristics. The H7 alloy is mostly brittle due to the flat surfaces shown inside the blue circle in Figure 18A. Alloy H7 had the highest hardness and strength at 62.3 HRC and 1856 MPa, but also had the least extension of 0.3 mm, which demonstrates that the H7 alloy was one of the more brittle alloys.

The P8-X11 alloy displays a mixed mode fracture with mainly brittle characteristics, but indicating microscopic ductility regions shown in the red circle in Figure 18D. The P8-X11 had the largest extension at about 4.86 mm, which implies that this alloy has at least some limited ductility present. This explains why there are pockets of microscopic ductility throughout the fracture surface. Although this data is not quantifiable, it is useful because hardfacing alloys tend to be nearly 100% brittle, so any level of ductility helps with crack prevention and therefore corrosion protection.

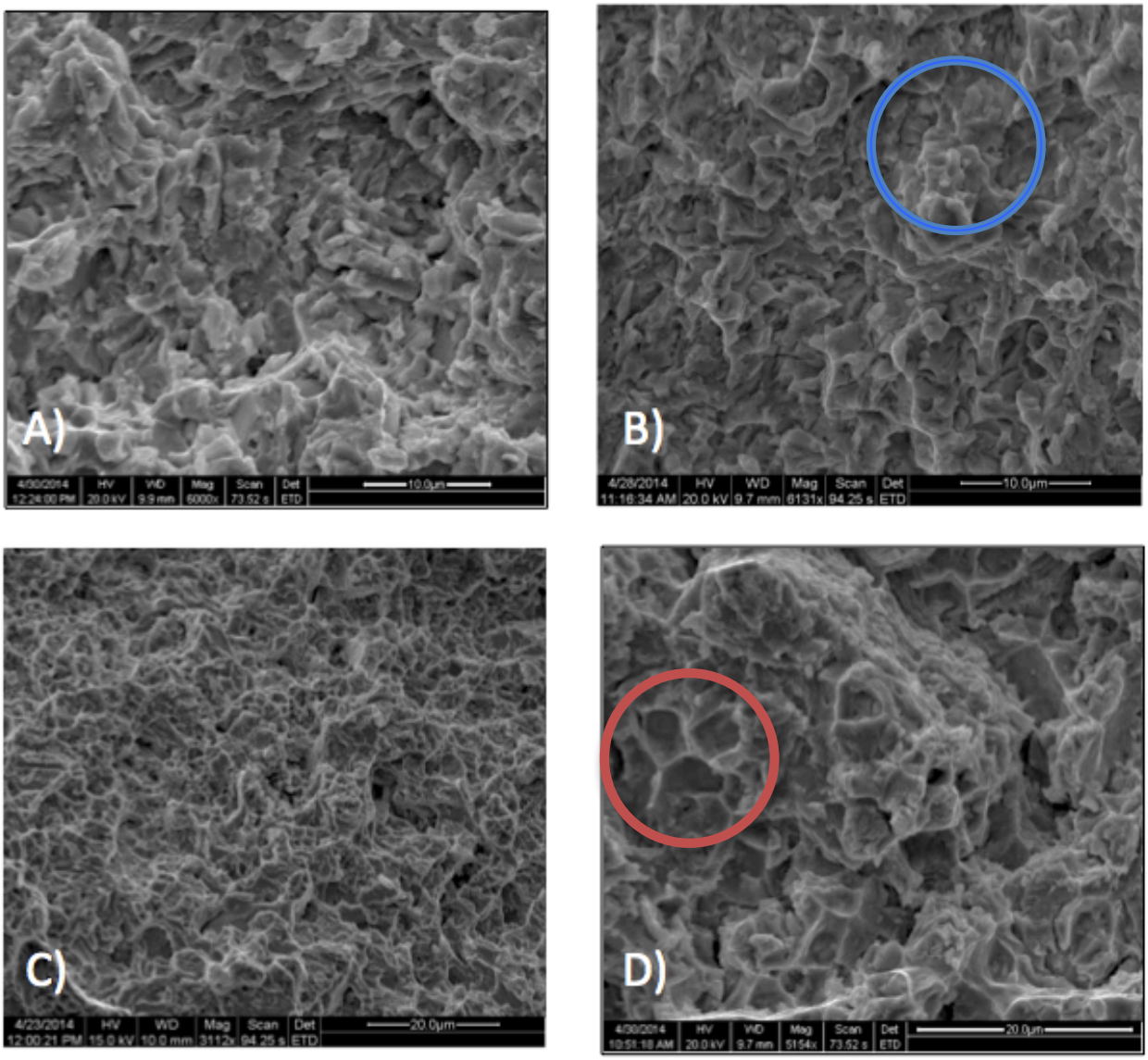

Figure 18: SEM images of the fracture surfaces of the four un-notched samples A) 350XT at 6000X magnification B) H7 at 6131X magnification C) P21-X9 at 3112X magnification and D) P8-X11 at 5154X magnification.

Microhardness

There was a correlation between hardness and strength values. The H7 hardfacing alloy had the highest strength and also had the highest hardness. The strength and hardness of this hardfacing alloy come from the microstrucural properties. This alloy's main application that it was designed for was hardfacing, so that is why it was hard and strong. On the other hand, the NS100 alloy had the lowest hardness and a relatively low strength comparatively. The main application

for this alloy was as a corrosion resistant weld overlay, which means that this alloy contains significantly more chromium, which aids in the corrosion protection. Since the main focus of this alloy is corrosion protection, it does not need to be designed to be as hard as the other alloys, such as the H7 alloy. The high standard deviation and high variance could be due to slight microstructural changes throughout the ingot sample, but this seems unlikely for the number of times the ingot was melted to ensure a homogeneous microstructure.

Conclusions

1. From the un-notched bend test, H7 hardfacing alloy had the highest strength at 1856 MPa with the smallest extension of 0.3 mm. P8-X11 hardfacing alloy had the lowest strength at 1583 MPa with the greatest extension of 4.86 mm.

2. SEM images of the fracture surface showed that the hardfacing alloys displayed a small level of microscopic ductility, which aids in crack prevention and corrosion protection.

3. There was a correlation between hardness values and strength values.

4. The notched bend test results were expected to be lower strength values due to the stress concentrations that were present in the V-shaped notch.

References

1. Freudenric, Craig H, Ph.D, and Jonathan Strickland. "How Oil Drilling Works." *How Stuff Works*. A Discovery Company, n.d. Web. 15 Oct. 2013.
2. "DRILLING EQUIPMENT." *Drilling Equipment Used for Purposes of Oil Extraction*. N.p., n.d. Web. 23 Nov. 2013. <http://www.flowtechenergy.com/Oilfield-Equipment/Drilling-Equipment/>.
3. Kilduff, Thomas F. "Other Methods of Surface Modification." *Engineering Materials Technology*. By James A. Jacobs. 5th ed. Columbus, Ohio: Prentice Hall, 2005. 412-13. Print.
4. "Hardfacing Alloys Introduction." *ASM International*. N.p., 1998. Web. 17 Oct. 2013.
5. "Corrosion Resistant Weld Overlay / Clad Welding." *Rode Welding Service*. N.p., n.d. Web. 18 Jan. 2014. <http://www.rodewelding.com/steel-fabrication/weld-overlay.asp>.
6. Rafa, Kyle. "The Effects of Carbon, Boron and Vanadium on the Microstructural Evolution and Hardness of Steel-based Hardfacing Alloys." *Materials Engineering Senior Project* (n.d.): 1-10. *California Polytechnic State University*. Web. 22 Oct. 2013.
7. "CLASSIFICATION OF HARDFACING ALLOYS." *ESAB*. N.p., n.d. Web. 22 Nov. 2013. <http://www.esabna.com/EUWeb/AWTC/Lesson8_12.htm>.
8. "Davis, J.R., Hardfacing, Weld Cladding, and Dissimilar Metal Joining." Vol. 6, *ASM International*. P 789-829, 1993. Web. 17 Oct. 2013.
9. "What Is Weld Overlay?" *Renown Oil & Gas LTD*. N.p., n.d. Web. 13 Jan. 2014. <http://www.renown-oil-and-gas.co.uk/wp-content/uploads/2012/01/Information-Sheet-What-Is-Weld-Overlay.pdf>.
10. Kuzniar, Renee. "The Effects of Heat Treatment on the Grain Growth, Phase Evolution, and Hardness of Newly Developed Steel-based Hardfacing Alloys for Industrial Applications." *Materials Engineering Senior Project* (n.d.): 1-10. *California Polytechnic State University*. Web. 31 Oct. 2013.
11. "ROGTEC Magazine - Russian Oil & Gas Technologies - News, Reviews & Articles." *ROGTEC Magazine Russian Oil Gas Technologies Magazine*. N.p., 7 Jan. 2013. Web. 18 Jan. 2014. <http://www.rogtecmagazine.com/blog/new-non-metallic-hardbanding-improves-wear-resistance-in-non-mag-applications>.
12. "Superior Performance in Cutting, Welding and Hardfacing Products." *NANO 7 Ultra High Performance Crack-Free Alloy*. N.p., n.d. Web. 23 Nov. 2013. <http://www.broco-rankin.com/hardfacing/smoothbanding/nano-7-ultra-high-performance-crack-free-alloy/>.
13. "Hard-facing by Welding." *Deloro Stellite*. N.p., 2012. Web. 18 Jan. 2014. <http://www.stellite.de/ProcessesOutline/CoatingServices/HardfacingbyWelding/tabid/119/Default.aspx>.

14. "Controlling Weld Metal Dilution." *Repair and Maintenance Welding Handbook* 2 (n.d.): n. pag. ESAB. Web. 4 June 2014. <http://www.esab.com/france-benelux/fr/erc-login/upload/Handbook-R-M-XA00086820.pdf>.

15. "Laboratory 7: Bend Testing." Mechanical Metallurgy Laboratory, n.d. Web. 4 Dec. 2013. PDF.

16. "Journal of Materials Chemistry." *Electroactive Polymer Actuators with Carbon Aerogel Electrodes - (RSC Publishing)*. N.p., n.d. Web. 30 Jan. 2014. <http://pubs.rsc.org/en/content/articlelanding/2011/jm/c0jm01729a>.

17. "Flexure Test." *Flexure Test*. Instron, n.d. Web. 18 Jan. 2014. <http://www.instron.us/wa/applications/test_types/flexure/default.aspx>.

18. Menedez, Patricio F., Namin Barnes, and Kurtis Bell. "Welding Processes for Wear Resistant Overlays." *Journal of Manufacturing Processes* (2013): n. pag. *Science Direct*. Web. 18 Jan. 2014. <http://www.sciencedirect.com.ezproxy.lib.calpoly.edu/science/article/pii/S1526612513000807>.

19 "Bend Testing." *ASM International*. N.p., 2013. Web. 30 Nov. 2013. <PDF>.

20. "CONVERSION CHART OF VICKERS HARDNESS (HV) TO ROCKWELL C (HRC)." *Taylor Special Steels*. N.p., n.d. Web. 23 Jan. 2014. <http://www.taylorspecialsteels.co.uk/pages/main/conchart.htm>.

21. Peterson, R. E., and R. Plunkett. "Stress Concentration Factors." *Journal of Applied Mechanics* 42.1 (1975): 248. Web. 3 June 2014. <http://www.ewp.rpi.edu/hartford/~ernesto/Su2012/EP/MaterialsforStudents/Aiello/Roark-Ch06.pdf>.

Appendix A: SEM Fracture Surface Images

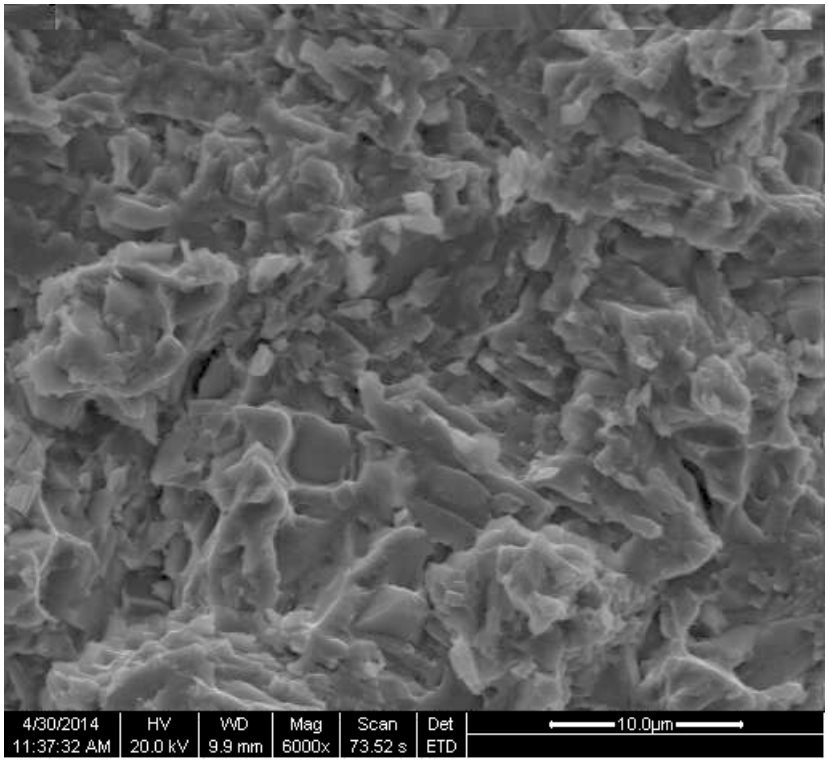

Figure 19: SEM image of fracture surface of 350XT alloy at 5000X magnification.

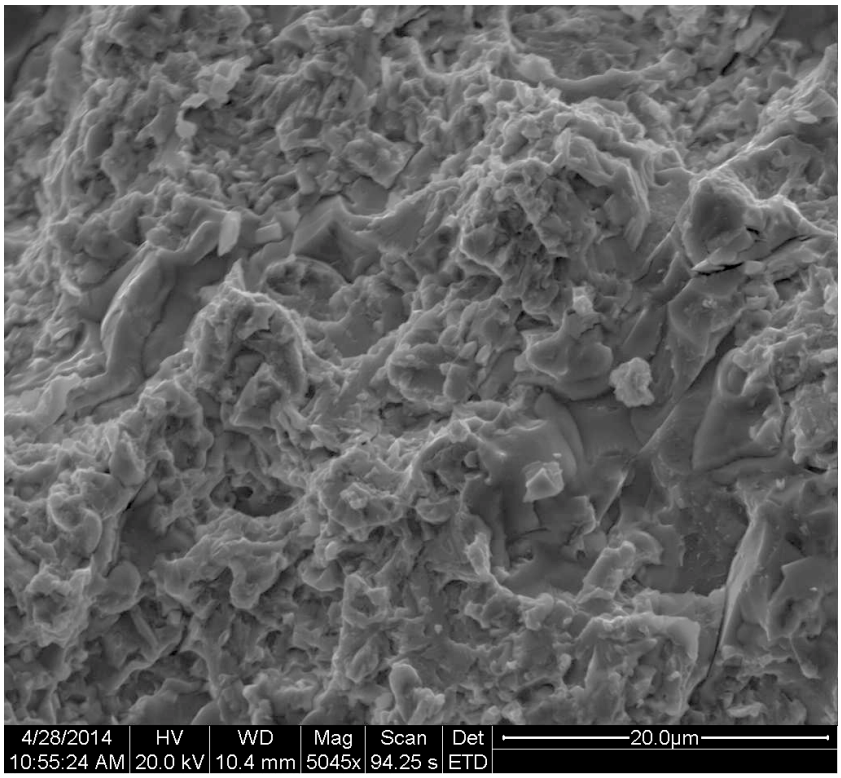

Figure 20: SEM image of fracture surface of H7 alloy at 5054X magnification.

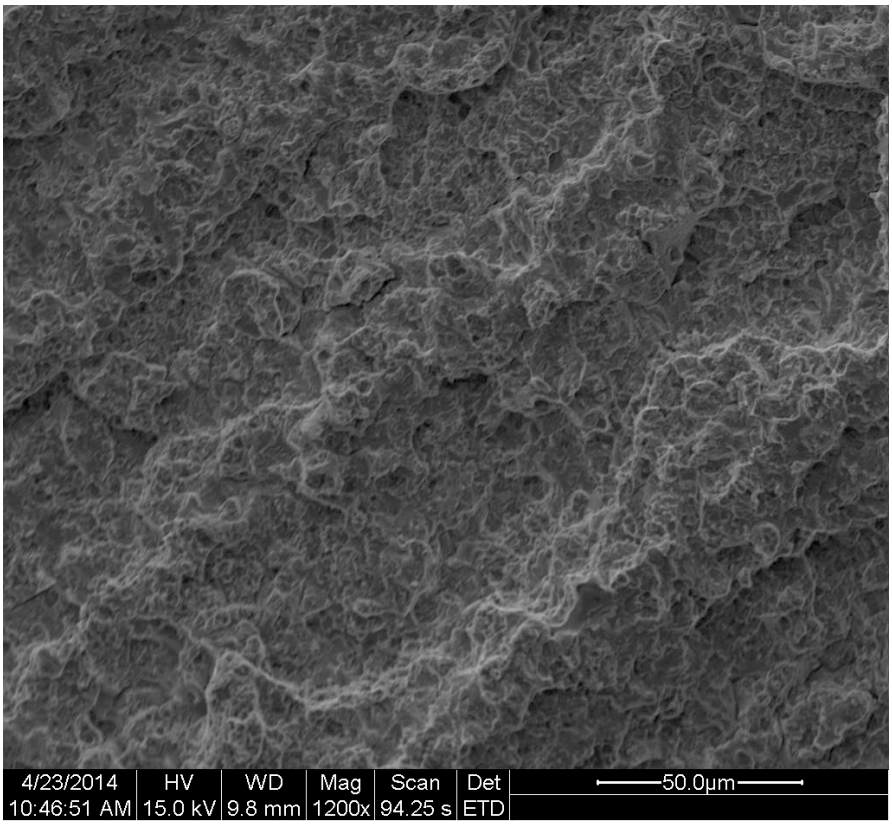

Figure 21: SEM image of the fracture surface of P21-X9 alloy at 1200X magnification.

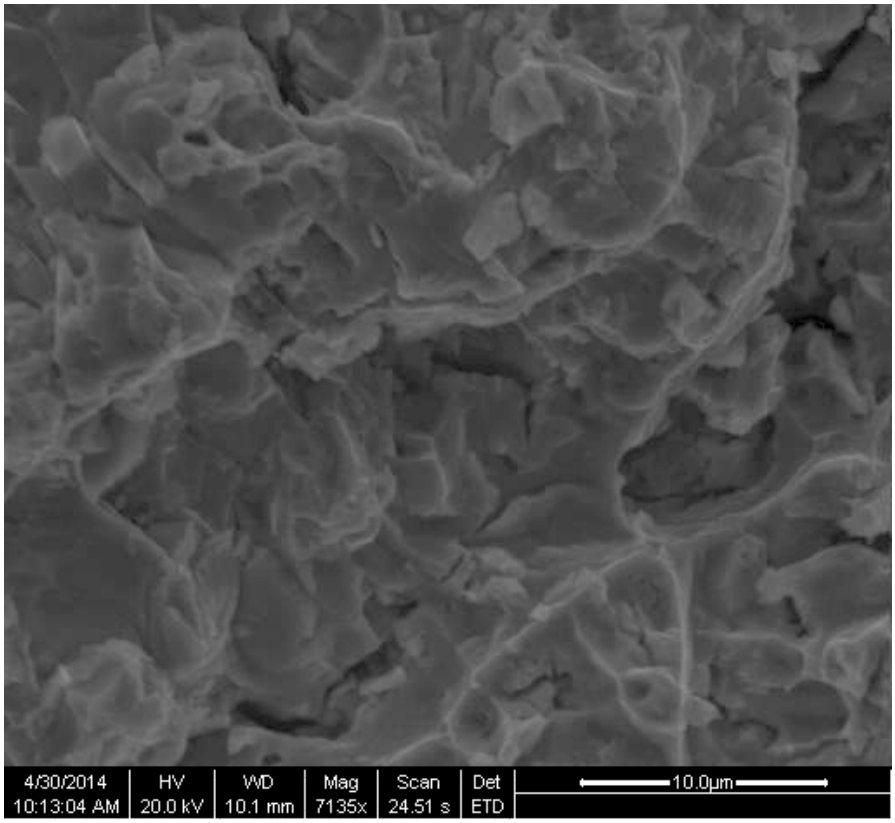

Figure 22: SEM image of the fracture surface of P8-X11 alloy at 7135X magnification.

Appendix B: Microhardness data

Table VIIII: Microhardness Values for all 6 Hardfacing Alloys

Sample	**Vickers**	**Sample**	**Vickers**
H7	802	P8-X11	343
H7	826	P8-X11	343
H7	802	P8-X11	356
H7	767.5	P8-X11	356
H7	826	P8-X11	336
H7	826	P8-X11	386
H7	779	P8-X11	258
H7	767.6	P8-X11	324
H7	826	P8-X11	330
H7	725	P8-X11	309.5
H7 AVG	**794.71**	P8-X11 AVG	**334.15**
350XT	826	AHB 35	526
350XT	586.5	AHB 35	458
350XT	779	AHB 35	458
350XT	802	AHB 35	458
350XT	813.5	AHB 35	490
350XT	813.5	AHB 35	490
350XT	736	AHB 35	463
350XT	813.5	AHB 35	507
350XT	757	AHB 35	501
350XT	677	AHB 35	677
350XT AVG	**760.4**	AHB 35 AVG	**502.8**
P21-X9	696	NS 100	320.5
P21-X9	659	NS 100	296
P21-X9	746	NS 100	285
P21-X9	609	NS 100	271
P21-X9	642	NS 100	296
P21-X9	677	NS 100	318
P21-X9	642	NS 100	298.5
P21-X9	633.5	NS 100	282.5
P21-X9	642	NS 100	282.5
P21-X9	625	NS 100	296
P21-X9 AVG	**657.15**	NS 100 avg	**294.6**

Table X: HRC Values for All Six Hardfacing Alloys

Sample	**Vickers AVG**	HRC
H7	795	62.3
350XT	760	60.9
P21- X9	657	56.8
P8-X11	334	35
AHB 35	503	49.8
NS 100	295	30.3